IEEE Access
Multidisciplinary ⋮ Rapid Review ⋮ Open Access Journal

Received May 9, 2022, accepted May 29, 2022, date of publication June 1, 2022, date of current version June 8, 2022.

Digital Object Identifier 10.1109/ACCESS.2022.3179493

Time-Modulated Patch Antennas With Tunable and Nonreciprocal Polarization Response

JAMES T. S. DO[1], JIAWEI ZANG[2], (Member, IEEE), ALEJANDRO ALVAREZ-MELCON[3], (Senior Member, IEEE), AND JUAN SEBASTIAN GOMEZ-DIAZ[1], (Senior Member, IEEE)

[1]Electrical and Computer Engineering Department, University of California at Davis, Davis, CA 95616, USA
[2]China Academy of Information and Communications Technology, Beijing 100191, China
[3]Communication and Information Technologies Department, Universidad Politecnica de Cartagena, Campus Muralla del Mar, Cuartel de Antigones, Cartagena, 30202 Región de Murcia, Spain

Corresponding author: Juan Sebastian Gomez-Diaz (jsgomez@ucdavis.edu)

This work was supported in part by the National Science Foundation with CAREER Grant ECCS-1749177, in part by the Ministerio de Economia y Competitividad of Spain, in part by the European Regional Development Funds under Grant PID2019-103982RB-C42, and in part by the National Natural Science Foundation of China under Grant 62001520.

ABSTRACT In this paper, we propose and demonstrate time-modulated patch antennas able to exhibit opposite polarization ellipticity when operated in transmission or reception, effectively leading to nonreciprocal polarization responses. To this purpose, we merge a patch antenna fed from four symmetrical sides with a low-frequency time-modulation scheme. This configuration exploits the photonic Aharonov Bohm effect to individually manipulate the phase of surface currents flowing along orthogonal directions on the antenna with the phase of the modulation signals. The polarization states of the radiated/received waves can easily be calculated using diagrams in the Poincaré sphere together with the phase difference of the modulating signals. Experimental results at 2.2 GHz demonstrate high conversion efficiency in the time-modulation process, isolation levels over 40 dB in transmission/reception mode, and tunability to generate/receive electromagnetic waves with arbitrary polarization ellipticity. Our findings may enable exciting applications in full-duplex communications as well as in polarimetric radar, sensing and imaging systems.

INDEX TERMS Time-modulation, nonreciprocity, patch antennas, polarization.

I. INTRODUCTION

Recent years have witnessed the quick emergence of magnetless nonreciprocity [1], [2] and the development of a wide variety of integrated, CMOS-compatible microwave devices such as circulators [3]–[7], isolators [8], [9], and nonreciprocal filtering structures [10]–[13]. Additionally, ultrathin metasurfaces have recently been put forward to manipulate the refraction and transmission properties of free-space propagating beams in a nonreciprocal manner [14]–[29]. For instance, they have been demonstrated to behave as serrodyne frequency translators employing a sawtooth waveform as modulation signal [14]. Space-time coding metasurfaces have recently enabled simultaneous control of electromagnetic waves in both spatial direction and harmonic power distribution [15]–[18]. Similar responses have been obtained using time-modulated Huygens metasurfaces by independently tailoring in time and space the magnetic and electric dipoles that compose each unit-cell of the structure [19]. Nonreciprocal beam scanning for fixed directions in space has theoretically been investigated by inducing space-time photonic transitions in spatiotemporally modulated surfaces [20] and a more general form of the classical Snell's relation not bounded by Lorentz reciprocity was also derived [21]. Time-modulated gradient metasurfaces [22]–[28] provide nonreciprocal beam steering, focusing, and polarization functionalities. A recent review on this topic can be found in [29].

In the context of antennas [30], [31], nonreciprocal responses able to provide large isolation between reception and transmission at desired directions in space have the potential to significantly impact radar, sensing and wireless communication systems, handle unwanted interferences or jamming signals, and enhance the performance of certain

The associate editor coordinating the review of this manuscript and approving it for publication was Shah Nawaz Burokur.

class of sensors. Early attempts employed ferrites to break reciprocity [32], [33], leading to antennas with limited efficiency and whose tunable responses required the presence of bulky and lossy magnets that are not compatible with integrated circuits. Magnetless spatiotemporal modulation techniques [2], [34] have been applied to realize non-reciprocal leaky-wave antennas by exploiting space-time transitions between guided and leaky modes [35]–[37]. Unfortunately, leaky-wave antennas may suffer from challenges in terms of size, complexity, efficiency, and dispersive beam scanning behavior that limit their use in practical applications. Recently, time-modulated phased-array antennas were demonstrated to exhibit drastically different radiation patterns in transmission and reception [38]. There, each antenna element is time-modulated with a low-frequency signal f_m enabling controllable nonreciprocity: the phase of transmitted signals follows the phase of the modulating signal φ_m whereas the phase of the received signal follows the opposite one, i.e., $-\varphi_m$. Even though the magnitude of the radiation pattern of each element is reciprocal, this approach permits to impose different phase profiles for the overall antenna array when transmitting or receiving. As a result, isolation levels over 40 dB were demonstrated at desired directions in space [38]. Other approaches to construct nonreciprocal antennas rely on connecting nonreciprocal components – such as filters or phase-shifters – with the radiating elements [39]–[42].

To date, nonreciprocal antennas have been mostly focused on controlling the magnitude of transmitted/receiving fields with a fixed polarization state. Antennas with nonreciprocal response at the polarization level may pave the way to a new set of polarimetric functionalities [43]–[45] and applications in radar, sensing, and imaging, as well as in communication systems. It should be stressed that these antennas would be quite different than polarization reconfigurable antennas widely explored in recent years [46]–[51]. Even though these structures are tunable and thus can change their polarization state (using switches, diodes, MEMS, etc.), they are always reciprocal because the polarization of transmitted and received waves at any instant are identical. For instance, consider the case of an antenna continuously radiating right-handed elliptically polarized waves. Upon reflection on a metallic screen, the wave handedness changes and thus it cannot be received by the same antenna. This challenge has led to an increased complexity in polarimetric systems.

In this contribution, we propose and experimentally demonstrate time-modulated patch antennas able to exhibit nonreciprocal polarization ellipticity when operating in reception or transmission, as illustrated in Fig. 1. A very preliminary theoretical study on this subject by the authors appeared in a recent conference [52]. The antenna relies on time-modulating orthogonal surface currents induced in a patch using low frequency signals with controllable phases. Measured data confirms isolation over 40 dB at the broadside direction and tunability to generate and receive electromagnetic waves with arbitrary ellipticity. The proposed time-modulation approach is general, as it can be applied to any resonant antenna element able to support surface currents in orthogonal directions.

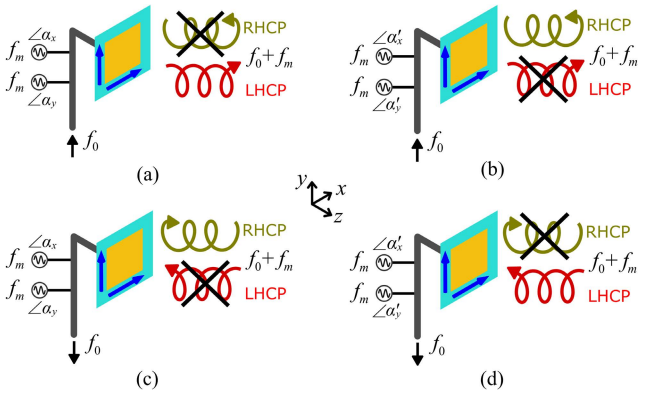

FIGURE 1. Time-modulated antenna with nonreciprocal polarization ellipticity in transmission and reception. The antenna is time-modulated with two low-frequency (f_m) signals with phases φ_x and φ_y that interact with x- and y- directed surface currents, respectively. Manipulating the phase difference between the modulation signals permits to control the polarization state of the transmitted/receiving fields in a nonreciprocal manner. In the left column, the phase shift is set to $\Delta\varphi^t = \varphi_x - \varphi_y = -90°$ and the antenna radiates LHCP waves and simultaneously receives RHCP waves. In the right column, the phase shift is set to $\Delta\varphi^t = \varphi_x - \varphi_y = +90°$ and the antenna radiates RHCP waves and receives LHCP waves.

This paper is organized as follows. Section II describes the operation principle of time-modulated antennas with nonreciprocal polarization ellipticity. Section III proposes a specific implementation of these structures based on a modified patch antenna controlled with low-frequency modulation signals. Sections IV and V describe the simulation and experimental set-up, respectively. Section VI presents numerical and measured data to validate the nonreciprocal and tunable response of the proposed antennas. Finally, Section VII concludes the paper.

II. OPERATION PRINCIPLE

The operation principle of time-modulated antennas with nonreciprocal polarization ellipticity is illustrated in Fig. 1. The approach relies on the photonic Aharanov-Bohm effect [38] to impose opposite phase profiles on orthogonal surface currents induced on the antenna when it is operated in transmission and reception. Let us consider an antenna that resonates at $f_0 + f_m$ and that supports orthogonal and *symmetric* surface currents along the x- and y- directions (Fig. 1). The antenna is time-modulated along these directions with signals exhibiting identical low-frequency f_m but different phases φ_x and φ_y, respectively. Exploiting certain design considerations in the antenna structure (see Section III), it can be enforced that the time-modulation process yields perfect frequency conversion between an incoming RF signal with frequency f_0 and any desired harmonic ($f_0 \pm nf_m$). For simplicity, we will consider here conversion with the upper side first harmonic $n = +1$ [38]. In this scenario, the antenna will up-convert a signal at f_0 to the frequency $f_0 + f_m$ (i.e., $f_0 \rightarrow f_0 + f_m$) that will then be radiated to free space. The fields radiated along the x- and y- directions will exhibit identical amplitude but

different phases. Such phases are given by

$$\angle \mathrm{E}_x^{\mathrm{t}} \propto (\varphi_{\mathrm{RF}} + \varphi_x), \quad \angle \mathrm{E}_y^{\mathrm{t}} \propto (\varphi_{\mathrm{RF}} + \varphi_y) \tag{1}$$

where $\angle \mathrm{E}_{\mathrm{p}}^{\mathrm{t}}$ denotes the phase of the electric fields transmitted at $f_0 + f_m$ along the $p = \{x, y\}$-direction and φ_{RF} is the phase of the RF signal at f_0. The phase difference between the x- and y- directed radiated fields is given by $\Delta\varphi^t = \varphi_x - \varphi_y$. As a result, the radiated wave will have a polarization state determined by an ellipticity $2\chi^t = \Delta\varphi^t$ and an azimuthal angle $\psi = 45°$ [30], [31]. The latter appears because this antenna configuration always radiates both x and y components of the electric field with identical amplitude.

In reception mode, the antenna will receive fields oscillating at $f_0 + f_m$ along the x- and y- directions and will down-convert them to the frequency f_0 (i.e., $f_0 + f_m \rightarrow f_0$). The phases of the received signals are

$$\angle \mathrm{E}_x^{\mathrm{r}} \propto \left(\varphi_x^{\mathrm{FS}} - \varphi_x\right), \quad \angle \mathrm{E}_y^{\mathrm{r}} \propto (\varphi_y^{\mathrm{FS}} - \varphi_y) \tag{2}$$

where $\angle \mathrm{E}_{\mathrm{p}}^{\mathrm{r}}$ denotes the phase of the fields down-converted to f_0 along the p-direction, and φ_p^{FS} is the phase of the impinging free-space wave at $f_0 + f_m$ along p. The received fields $\mathrm{E}_x^{\mathrm{r}}$ and $\mathrm{E}_y^{\mathrm{r}}$ interfere within the antenna, leading to a maximum reception when they are in phase, i.e., $\angle \mathrm{E}_x^{\mathrm{r}} = \angle \mathrm{E}_y^{\mathrm{r}}$, and minimum reception when they are out of phase, i.e, $\angle \mathrm{E}_x^{\mathrm{r}} = \angle \mathrm{E}_y^{\mathrm{r}} + \pi$. The phase difference between the x- and y- directed fields imparted by the time-modulated antenna is given by $\Delta\varphi^r = \varphi_y - \varphi_x = -\Delta\varphi^t$. As a result, the antenna will optimally receive waves with a polarization state determined by an ellipticity $2\chi^r = \Delta\varphi^r$ and an azimuthal angle $\psi = 45°$ [30], [31]. It is thus evident that $\chi^t = -\chi^r$, which highlights the nonreciprocal polarization ellipticity between reception/ transmission responses of this type of antennas.

It is instructive to employ the Poincaré sphere to explore the polarization response of antennas [30], [31]. The Poincaré sphere, illustrated in Fig. 2, represents polarized electromagnetic waves using the Stokes parameters (S_1, S_2, S_3) [30], [31] as the Cartesian coordinates, i.e.,

$$x = S_1 = \cos(2\chi)\cos(2\psi), \tag{3}$$

$$y = S_2 = \cos(2\chi)\sin(2\psi), \tag{4}$$

$$z = S_3 = \sin(2\chi), \tag{5}$$

where S_1 is associated to horizontal/vertical linearly polarized (LP) light, S_2 is related to $\pm 45°$ LP light, and S_3 correlates to circularly polarized (CP) light [30], [31]. Any polarized light represents a point on the surface of the sphere. Let us now consider the proposed antenna operating in transmission. By manipulating the relative phase $\Delta\varphi^t$ with a phase shifter, the proposed antenna is capable of radiating waves with any desired ellipticity– as highlighted in the green circle plotted over the Poincaré sphere in Fig. 2. For instance, a phase shifter operated in a state Q will lead to a specific relative phase $\Delta\varphi_q^t$ and thus the antenna will radiate waves with an ellipticity χ_q^t. The same antenna operated in reception will optimally receive waves with an opposite ellipticity

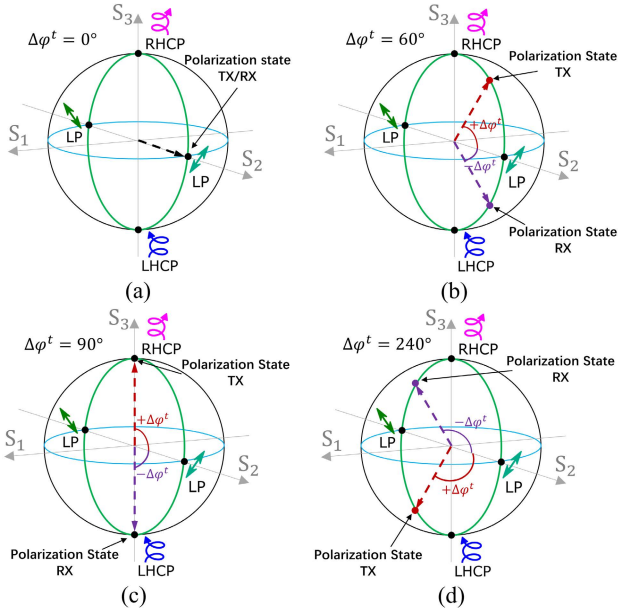

FIGURE 2. Polarization states radiated/received by the antenna mapped into the Poincaré sphere. The states are shown using ellipticity and azimuthal angles measured from the equator and S_1 axis, respectively. Results show the polarization state of the waves transmitted and received by the proposed antenna for different phase shift $\Delta\varphi^t$ between the time-modulating signals: (a) $\Delta\varphi^t = 0°$; (b) $\Delta\varphi^t = 60°$; (c) $\Delta\varphi^t = 90°$; and (d) $\Delta\varphi^t = 240°$. The antenna radiates and receives waves with arbitrary ellipticity at azimuthal angle $\psi = 45°$, i.e., the green circle along the sphere surface defined in the $S_2 - S_3$ plane. Polarization ellipticity during transmission and reception has same magnitude but different phase, which translate to opposite states in the Poincaré sphere.

$\chi_q^r = -\chi_q^t$. Fig. 2 illustrates such behavior for four different phase shifts $\Delta\varphi^t$ between the low-frequency signals that modulate the patch antenna. Changing the state of the phase shifter to obtain a relative phase $\Delta\varphi^t = \{0, \frac{\pi}{2}, \pi, -\frac{\pi}{2}\}$, will lead to a nonreciprocal antenna that radiates electromagnetic waves with a polarization state {+45° LP, right-handed CP (RHCP), −45° LP, left-handed CP (RHCP)} and receive waves with opposite ellipticity, i.e., {+45° LP, LHCP, −45° LP, LHCP}.

It should be noted that manipulating the relative phases of the low-frequency modulation signals does not suffice to cover all possible states of the Poincaré sphere. To obtain such response, the amplitude of the surface currents induced along orthogonal directions within the antenna should simultaneously be controlled upon time-modulation.

III. TIME MODULATED PATCH ANTENNA WITH NONRECIPROCAL POLARIZATION CONTROL

In this section, we propose a specific implementation to realize time-modulated patch antennas with nonreciprocal polarization ellipticity. The antenna details are shown in Fig. 3. Specifically, an RF signal (f_0) is input from port 1 (P_1) and flows along the microstrip lines on the top layer to feed a square patch from four sides. Quarter-lambda transformers are implemented in the microstrip lines to guarantee impedance matching between the power divided t-lines and the patch antenna. Additionally, four coplanar

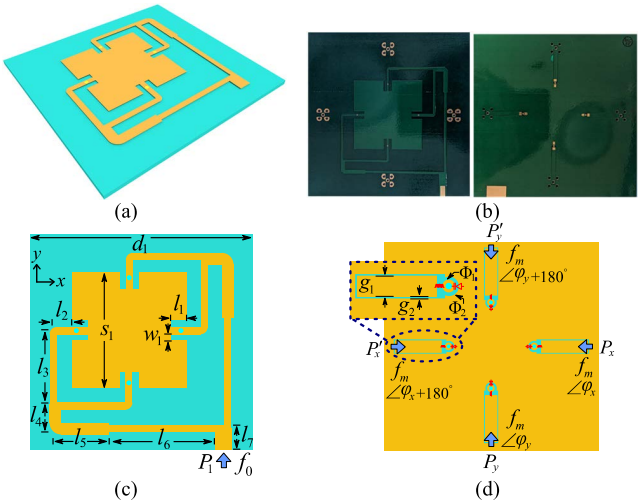

FIGURE 3. Layout of the proposed time-modulated patch antenna with nonreciprocal polarization response. (a) 3D view. (b) Photographs of a manufactured prototype. (c) Top view. RF signal is fed from port 1 (P1) and symmetrically split to feed the four sides of a square patch. (d) Bottom view depicting the feeding network for time-modulated signals. Each port is composed of a CPW terminated into a via-hole that connects to the top patch. A varactor and an inductor connect the via-hole and the CPW. A rogers RT/duroid 5880 substrate with a thickness of 1.575 mm, a relatively dielectric constant of 2.2, and a loss tangent of 0.0009 is used. The antenna dimensions (mm) are: $d_1 = 110$, $l_1 = 7, l_2 = 8.2, l_3 = 30.5, l_4 = 8.4, l_5 = 15.5, l_6 = 49.4, l_7 = 11.7, w_1 = 2, s_1 = 46, g_1 = 2.6, g_2 = 0.2, \Phi_1 = 0.5, \Phi_2 = 1$.

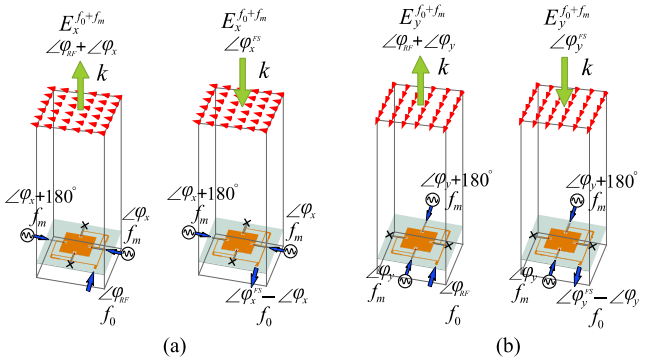

FIGURE 4. Numerical simulation setup employed to illustrate the phase response of the proposed antenna in transmission and reception. (a) Time-modulation is only applied along the x-axis. (b) Time-modulation is only applied along the y-axis.

waveguides (CPWs) are located in the bottom ground plane. Each CPW is loaded with a varactor (SMV1235 from Skyworks Solutions Inc.) and is connected to the microstrip line on the top layer through a metallic via. All varactors are reversely biased by DC voltage. Low frequency (f_m) modulation signals and DC bias voltages are carried simultaneously within each CPW. For each modulation path, an inductor is employed as an RF choke to improve the isolation between the RF and modulation signals. Details of the configuration are shown in Fig. 3(c) and Fig. 3(d). Even though all modulation signals oscillate at the same frequency f_m, their phase distribution may vary across the different CPW. Specifically, ports located across the x-axis, P_x and P'_x, are fed with f_m signals with phases φ_x and $\varphi_x + \pi$, respectively. A phase difference of 180° is imposed between these modulation signals to enforce efficient frequency conversion in the nonlinear process by exploiting the even and odd modes of the antenna at f_0 and $f_0 + f_m$, respectively. This process is described in detail in [38]. Similarly, ports located along the y-axis, P_y and P'_y, are fed with f_m signals with phases φ_y and $\varphi_y + \pi$, respectively. The final optimal dimensions of the proposed time modulated patch antenna are given in the caption of Fig. 3.

The polarization characteristics of the fields radiated and received by this antenna can be controlled through the phases φ_x and φ_y exploiting the orthogonality of the surface currents induced on the patch. This process is illustrated in Fig. 4. Let us first consider that the modulation signals are applied only along the x-oriented CPWs located in the ground plane, as shown in Fig. 4(a). In the transmission mode, the antenna will radiate purely x-polarized electric fields oscillating at $f_0 + f_m$ with a phase proportional to $\varphi_x + \varphi_{RF}$. In this process, symmetrical RF signals fed the patch from opposite directions in the x-axis, exciting the patch even mode and generating a surface current null at the center of the structure [38]. The reflected signals are then up-converted to two out-of-phase signals at frequency $f_0 + f_m$ that excite the common odd mode of the patch, leading to the efficient radiation of x-polarized fields. Note that even mode harmonics cannot be radiated for the patch, as the antenna effectively impose a virtual open circuit for even harmonics generated by the varactors, i.e., $f_0 + pf_m$ with $p = \pm 2, 4, 6 \ldots$ We remark that y-polarized fields cannot be radiated in this case as the lack of time modulation leaves an even mode (virtual open circuit) along that direction. In reception, an incoming wave with frequency $f_0 + f_m$ and phase φ_x^{FS} impinges on the antenna and excites the resonant odd mode of the patch. Then, time-modulation along the x-axis down converts the signal to the guided even mode, with frequency f_0 and phase $\varphi_x^{FS} - \varphi_x$, that is routed to the exit port. Similar considerations can be made when the antenna is modulated along the y-axis and no modulation is applied along the x-direction, as illustrated in Fig. 4(b). In the case that the antenna is simultaneously time-modulated along the x and y axis, the low cross-coupling between orthogonal directions in a patch structure (<-25 dB) guarantees an independent control of the x- and y- polarized generated and received fields.

IV. SIMULATION SETUP

The proposed antenna is first designed and simulated in the linear regime using ANSYS HFSS (bottom-left inset of Fig. 5). In the model, lumped ports normalized to 50 Ω are employed in the position in which the varactor diodes and lumped inductors will be placed. In this 3D simulation, the antenna is placed in a periodic environment using two Floquet ports associated to the fundamental TE and TM modes at the broadside direction. This approach permits to obtain the amplitude and phase of the fields radiated

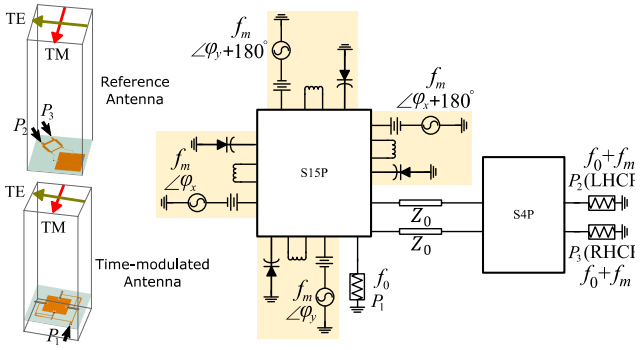

FIGURE 5. Nonlinear circuit simulation of the transmission/reception of electromagnetic waves at broadside between the proposed time-modulated antenna (inset bottom left) and a reference antenna (inset top left) described in Appendix I. The response of the antennas has been first obtained using numerical simulation assuming that the structures are placed in a periodic environment. Their linear response has then been imported into the circuit simulator and are shown in the figure as the box S15P for the time-modulated antenna and box S4P for the reference antenna. The two antennas are connected through transmission lines (characteristic impedance of 120π) that models the propagation of electromagnetic waves for the fundamental TE and TM Floquet modes [53]. The circuit is simulated using large signal scattering parameters.

by antenna, as detailed elsewhere [53]. Even though this simulation accounts for an infinite two-dimensional array of patch antennas, the dimensions of the unit-cells ensure a negligible cross-coupling at the targeted broadside direction. The linear S-parameters of the 3D model are then exported to the circuit simulator Keysight ADS to perform large signal S-parameter (LSSP) simulations. In the nonlinear circuit, the varactor diode and lumped inductor models are imported from the vendors and connected to the lumped ports of the antenna. The model is then explored to maximize the radiation efficiency, optimizing the modulation frequency ($f_m = 320$ MHz), modulation amplitude $M = 0.36$, and DC bias applied to the varactors ($V = 1.53$ volts) as described in [38].

To explore the response of the proposed time-modulated antenna, three different reference antennas will be employed. First, a common patch antenna is employed to calibrate the system and extract the overall loss in the radiation process [38]. Second, a linearly polarized horn-antenna is employed to explore the phase variations of the different field components radiated by the time-modulated antenna. And third, a reference patch antenna has been designed in HFSS and fabricated integrating a 90° hybrid coupler to independently control the LHCP and RHCP components of the radiated/received waves. This antenna, described in detail in Appendix I, will permit exploring the polarization response of the proposed time-modulated device.

Fig. 5 illustrates the ADS circuit model employed to interconnect the time-modulated antenna with the reference antenna described in Appendix I. Interchanging such reference antenna with another one (i.e., a patch or a horn antenna) simply requires updating the S parameters that describe the reference device. To simulate free-space propagation along the broadside direction that connect both antennas–assuming they are perfectly aligned– the orthogonal TE and TM Floquet modes from both linear antenna models are connected using transmission lines with a characteristic impedance of $Z_0 = 120\pi\,\Omega$. In the model, port 1 is assigned to the RF signal that feeds the time-modulated antenna whereas ports 2 and 3 are related to the LHCP and RHCP components of waves radiated/received by the linear reference antenna. The entire set-up is then simulated using LSSP, which measures nonlinear transmission/reception of fields between the time-modulated and reference antennas in a similar fashion as the frequency offset mode of a performance network analyzer (PNA). This setup permits to analyze the amplitude and phase of all field components radiated and received by the antennas under test.

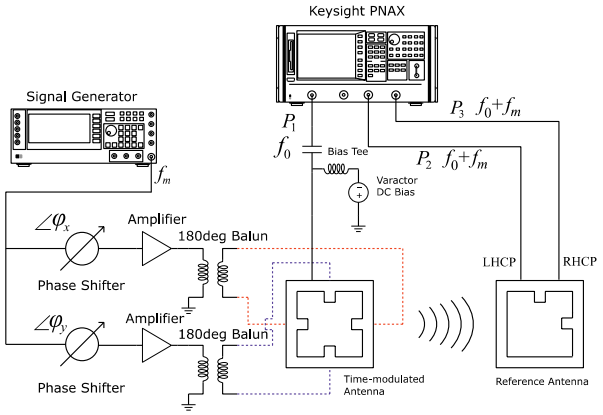

FIGURE 6. Measurement setup to characterize the transmission response of the proposed time-modulated antenna. A PNAX excites the antenna at f_0 whereas a signal generator provides the modulation signal f_m, which is split into two signals using a power divider. Phase shifters are then employed to manipulate the phases of the modulation signals whereas 180° baluns provide the required out of phase signals. The reference antenna (see Appendix I) is aligned at the normal direction of the modulated patch and split the received signal into LHCP and RHCP components that are then routed toward ports 2 and 3 of the PNAX.

V. EXPERIMENTAL SETUP

Fig. 6 shows an overview of the proposed experimental set-up. In all cases, microwave absorbers (not shown) are located around the antenna to minimize unwanted scattering. In the proposed set-up, a 4-port Keysight PNAX N5247A is used to simultaneously control the proposed time-modulated patch antenna as well as the reference antenna, providing quantitative information in amplitude and phase of the radiated fields. In this work, we will focus on the broadside radiation to explore the antenna polarization response. Note that a single time-modulated antenna element provides a reciprocal radiation pattern in amplitude [38] and therefore, obtaining radiation pattern is not an objective of this work. Prior to measurements, a standard short-open-load-through (SOLT) calibration is applied [30], [31]. Time-modulation signals oscillating at $f_m = 320$ MHz are obtained with a Hewlett Packard E4433B signal generator and fed to the antenna CPWs. Varactors are biased with 1.53 volts obtained from a standard DC voltage source. Power amplifiers and

Mini-Circuits ZXPHS-431 phase shifters are employed to obtain the desired amplitude and to impart phase shifts φ_x and φ_y to the modulation signals, respectively. Along each direction, Mini-circuits TCM2-33WX baluns impose the 180° phase different to the modulation signals.

In transmission mode, the PNAX is configured using the frequency offset mode so that the receivers (P2 and P3 in Fig. 6) are set to measure a swept signal with frequency f_0+f_m (2.1-2.3 GHz) while the transmit port (P1) frequency is swept at f_0 (1.781-1.981 GHz). The 10 MHz reference oscillators of the PNAX and signal generator are coupled together to phase lock the signals of the instruments. In reception, the PNAX is also configured in the offset mode but feeding now the reference antenna with a signal frequency $f_0 + f_m$ (2.1-2.3 GHz) through ports 2 and 3 and setting the receiver in port 1 to measure signals at $f_0 \sim$ 1.781-1.981 GHz.

VI. TUNABLE NONRECIPROCAL RESPONSE OF TIME-MODULATED ANTENNAS

This section explores the performance of the proposed antenna and its use in a simple communication system. The antenna is first characterized in terms of matching, efficiency, and ability to independently control the polarization of radiated fields along orthogonal directions. Then, nonreciprocal polarization in transmission/reception is demonstrated versus frequency, obtaining isolation levels >40 dB. Finally, we will show how the antenna radiates and receives fields with any desired ellipticity while maintaining its nonreciprocal behavior.

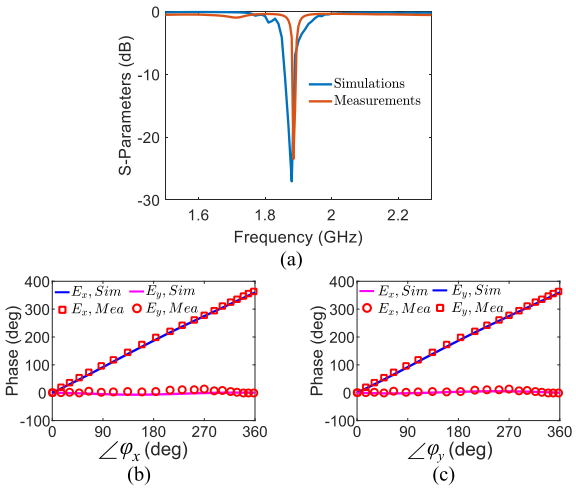

FIGURE 7. Electromagnetic response of the proposed time-modulated antenna. (a) Scattering parameters upon time-modulation. (b)-(c) Simulated (solid lines) and measured (markers) phase of the x- and y- components of the radiated electric field versus the phase of the modulation signals: (a) φ_x, keeping $\varphi_y = 0°$; and (b) φ_y, keeping $\varphi_x = 0°$. Results confirm independent phase control of orthogonal radiated fields through the phase of the signals that modulate the path antenna.

A. CHARACTERIZATION OF TIME-MODULATED ANTENNAS

Fig. 7(a) shows the measured scattering parameter S_{11} of the antenna upon time-modulation. Results confirm an excellent matching at the design frequency of 1.89 GHz. At that frequency, the input signal is up-converted to 2.21 GHz and radiated to free-space. To verify that this is indeed the case, we employed a standard patch antenna as reference antenna in the experimental schematic shown in Fig. 6 – see [38] for additional details. Strong radiation toward broadside direction is confirmed at 2.21 GHz with a total of ∼3 dB of loss with respect to a common patch [30], [31]. Such losses arise due to (i) presence of non-ideal varactors, capacitors, and power dividers; and (ii) frequency conversion to unwanted harmonics. The amount of loss and associated loss mechanisms are comparable to those found in time-modulated antennas that do not exhibit polarization control [38].

To explore the polarization response of the antenna, we employed a linearly polarized horn as a reference antenna in our experimental set-up. The antenna is aligned with respect to the time-modulated patch and carefully rotated to only receive x- or y-directed fields. Fig. 7(b) [Fig. 7(c)] shows measured and simulated phases of the x-component [y-component] of the received electric fields when the phase ϕ_x [ϕ_y] of the modulating signals is varied using the phase-shifter and the orthogonal one is set to zero. For simplicity, the phase reference of all signals transmitted in this simple channel has been set to zero for a zero value of the phase shift. Measured data confirm that the phase response of the y polarized electric field component changes linearly with the phase φ_y of the time-modulated signal directed along the y-axis, while it remains unchanged versus the phase of the low-modulation signal along the x-axis, φ_x. Similar response can be obtained for x-polarized radiated fields with respect to the φ_x and φ_y phases, respectively. This study demonstrates that the phase of each field component can be controlled in an independent manner with the phase of the corresponding time-modulating signal.

B. NONRECIPROCAL RESPONSES IN POLARIZATION

Fig. 8 explores the nonreciprocal polarization response of time-modulated antennas versus frequency when transmitting and receiving CP waves. This scenario is explored experimentally using the schematic shown in Fig. 6, employing the patch antenna combined with the 90° hybrid coupler as reference device (see Appendix). This structure is particularly useful to isolate the LHCP and RHCP components of the fields, and it is applied here to experimentally explore the transmission and reception of RHCP and LHCP radiation and to demonstrate isolation at the polarization level.

The top row of Fig. 8 plots the normalized response of the time-modulated antenna in transmission. In the left (right) panel, the antenna is configured to radiate a RHCP (LHCP) wave by setting the phase difference between the time-modulating signals to $\Delta\varphi^t = +90°$ ($\Delta\varphi^t = -90°$). The radiated signal is received by the reference antenna, where the LHCP and RHCP components of the

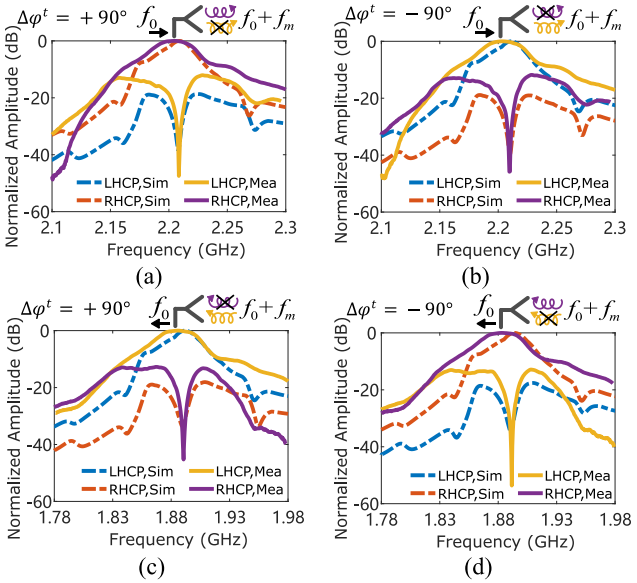

FIGURE 8. Nonreciprocal polarization response of the proposed antenna versus frequency. Measurement set-up follows Fig. 6. (a)-(b) Transmission mode. The time-modulated antenna radiates RHCP (LHCP) at $f_0 + f_m$ by enforcing a phase shift of $\Delta\varphi^t = +90°$ ($\Delta\varphi^t = -90°$) between the modulation signals. The radiated signal is received by the reference antenna and split into LHCP and RHCP components. (c)-(d) Reception mode. The reference antenna radiates first LHCP waves at $f_0 + f_m$ that are received by the time-modulated antenna and down-converted to f_0. The phase-shift between the modulation signals is set to $\Delta\varphi^t = +90°$ and $\Delta\varphi^t = -90°$ in panels (c) and (d), and therefore the antenna is tuned to receive LHCP and RHCP waves, respectively. Results are also computed when the reference antenna radiates RHCP waves. Simulation and measured data are shown using dashed and solid lines, respectively.

fields are separated and sent to the PNAX. At the targeted operation frequency of $f_0 + f_m = 2.21$ GHz, measured and simulation data confirm that the received signal is strongly RHCP (LHCP) whereas the LHCP (RHCP) component is over 40 dB smaller. The antenna response in reception mode is shown in the bottom row of Fig. 8. In the measurements, the reference antenna alternatively radiates RHCP and LHCP waves at $f_0 + f_m$. The antenna receives the waves and down converts them to guided waves at f_0. In the left (right) panel, the time-modulated antenna maintains a phase difference between time-modulating signals of $\Delta\varphi^t = +90°$ ($\Delta\varphi^t = -90°$), and therefore is tuned to receive LHCP (RHCP). Both simulated and measured results confirm that this is indeed the case, and that the antenna reception is maximum for LHCP (RHCP) waves, whereas orthogonal RHCP (LHCP) waves are received with over −40 dB of amplitude difference.

Nonreciprocity in polarization immediately follows from Fig. 8: setting $\Delta\varphi^t = +90°$, the antenna radiates RHCP waves and receives waves with the opposite ellipticity, i.e., LHCP; on the other hand, when $\Delta\varphi^t = -90°$, the antenna radiates LHCP waves and receives RHCP. Polarization isolation over 40 dB is obtained in all cases. Another remarkable feature is the high polarization purity exhibited by the antenna when configured to operate either in transmission or reception.

C. POLARIZATION CONTROL

In this subsection, we demonstrate the possibility of radiating and receiving fields with arbitrary polarization ellipticity (see highlighted green circle in Fig. 2) while keeping the nonreciprocal response. Such functionality can be obtained by manipulating the phases of the modulating signals, φ_x and φ_y.

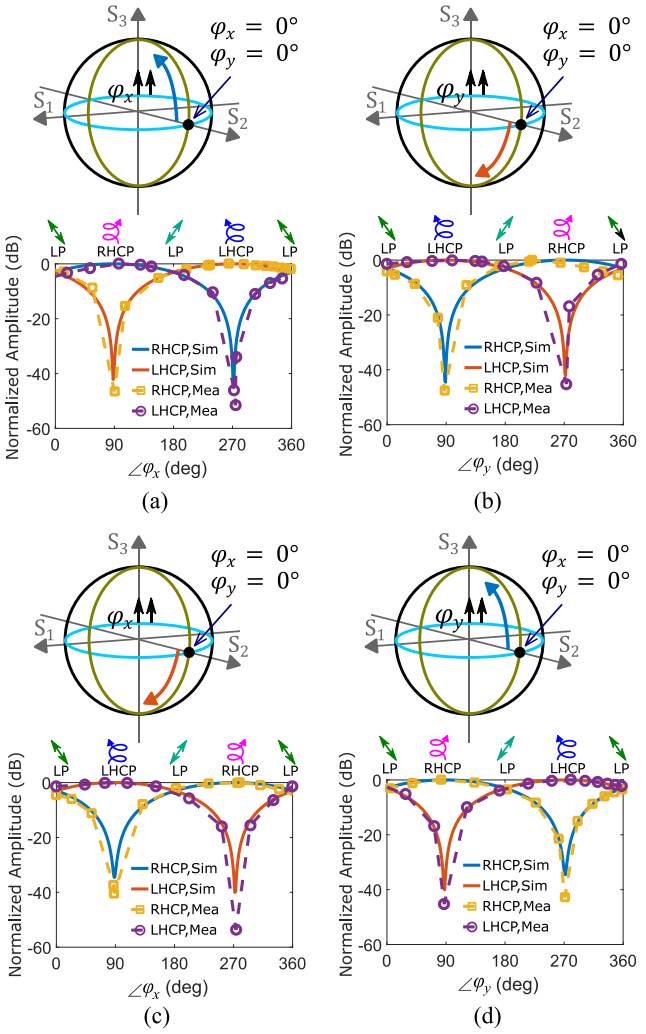

FIGURE 9. Manipulating the polarization of transmitted and received waves using the proposed time-modulated antenna. Measurement set-up follows Fig. 6. Results are calculated for transmission (top row) and reception (bottom row) modes for waves propagating in free space at $f_0 + f_m = 2.21$ GHz. On the left column, responses are plotted versus the phase φ_x of the time modulating signals keeping $\varphi_y = 0$, whereas on the right column, results are plotted versus φ_y keeping $\varphi_x = 0$. (a)-(b) Transmission mode. The time-modulated antenna radiates with a polarization state determined by the phase shift of the modulation signal (see upper axis for a reference). Signals received by the reference antenna are then decomposed into RHCP and LHCP components. (c)-(d) Reception mode. The reference antenna radiates first LHCP and then RHCP waves at $f_0 + f_m$ that are received by the time-modulated antenna and down-converted to f_0. Depending on the phase-shift between the modulation signals, the antenna is tuned to receive waves with a fixed polarization state (see upper axis of reference). Top insets illustrate how the polarization state of the transmitted/received waves evolve on the Poincare sphere as the phase of the time-modulated signals changes. Simulation and measured data are shown using dashed and solid lines, respectively.

Let us first consider the transmission mode. The PNAX is used to excite port 1 of the proposed antenna with a fixed frequency of $f_0 = 1.89$ GHz. The signal generator provides time modulated signals with frequency $f_m = 320$MHz to the antenna CPW ports. In Fig. 9(a), the phase shifter applied to the x-directed time-modulated signals is DC biased (Fig. 6) to provide an increasing phase shift φ_x while keeping $\varphi_y = 0$. This corresponds to moving counterclockwise in the highlighted states shown in the Poincaré sphere [see inset in Fig. 9(a)] that are radiated to free space. The RHCP and LHCP components of the signal received by the reference antenna are then routed to port 2 and 3 of the PNAX. When $\varphi_x = 0°$, the antenna is set to radiate $+45°$ linearly polarized waves and thus the receiver collects an equal amount of LHCP and RHCP component – each with a magnitude of -3 dB. As the phase shift φ_x increases, the transmitted RHCP component increases whereas the LHCP decreases. At exactly $\varphi_x = +90°$, the radiated signal acquires an almost pure RHCP state with an orthogonal LHCP component over -50dB lower. Increasing the phase φ_x further has the opposite effect, as the LHCP component gets larger while the RHCP decreases. Both components intersect again with an amplitude of -3dB when $\varphi_x = +180°$. At that point, the antenna radiates a $+45°$ linearly polarized state. Larger φ_x will decrease further the RHCP component and increase the LHCP, which will be maximum when $\varphi_x = +270°$. This state reveals that the orthogonal RHCP components is over -45 dB weaker and confirms the high polarization purity of the radiated signal. Greater φ_x phase shifts complete the circle along the Poincaré sphere. In all cases, excellent agreement has been found between simulations and measurements. Fig. 9(b) repeats this experiment but increasing the φ_y phase shift while keeping $\varphi_x = 0°$. In this scenario, the antenna again radiates electromagnetic states with all possible ellipticity values. The main difference is that the rotation over the radiated states in the Poincaré sphere is now clockwise [see inset in Fig. 9(b)] with respect to the phase φ_y.

In reception mode, the PNAX is first configured to feed the port 2 of the reference antenna with a frequency $f_0 + f_m = 2.21$ GHz while keeping port 3 terminated with a 50Ω load. Therefore, the antenna radiates a LHCP signal. In the experiment, we monitor the signal that has been received by the time-modulated antenna, down-converted to $f_0 = 1.89$ GHz and routed to port 1 of the PNAX. In Fig. 9(c) (solid blue line), we explore this situation versus the phase φ_x while keeping $\varphi_y = 0$. Due to the opposite ellipticity during transmission and reception, the antenna receives now electromagnetic waves with an ellipticity that is moving clockwise with respect to φ_x [see inset of Fig. 9(c)]. When the phase is set to $\varphi_x = \{0°, 180°\}$, the antenna receives the $\{+45°, -45°\}$ linearly polarized wave component of the transmitted RHCP wave that corresponds to a -3 dB amplitude. When $\varphi_x = 270°$, the received signal is maximum as the antenna is tuned to received LHCP waves. On the contrary, the received signal is over -40dB weaker when the antenna is configured to receive RHCP signals (by setting the phase $\varphi_x = 90°$) that are orthogonal to the radiated LHCP ones.

Next, the reference antenna is configured to radiate RHCP waves [solid red line in Fig. 9(c)]. To this purpose, its port 2 is loaded with 50Ω while its port 3 is fed by the PNAX with a frequency $f_0 + f_m = 2.21$ GHz. Simulated and measured data follow a similar pattern as described above: maximum (minimum) reception appears when the antenna is tuned to received RHCP (LHCP) with $\varphi_x = 270°$ ($\varphi_x = 0°$) whereas the $+45°$ ($-45°$) linearly polarized component of the transmitted RHCP is received when φ_x is set to 0° (180°). The experiment is repeated in Fig. 9(d) by varying now the phase φ_y while keeping $\varphi_x = 0°$. In such configuration, the antenna receives waves with an ellipticity moving counterclockwise with respect to φ_y (see inset). Experimental and simulated data show again an excellent agreement, demonstrating the ability of the antenna to receive waves with any polarization state and minimal cross-coupling while maintaining its nonreciprocal nature.

VII. CONCLUSION

This paper has introduced and experimentally demonstrated the concept of antennas exhibiting nonreciprocal polarization response when operated in transmission or reception. These structures support surface currents along orthogonal directions that exhibit opposite phase profile in transmission/reception upon time-modulation. As a result, the antenna is capable of radiating waves with any polarization ellipticity while simultaneously receiving waves with opposite ellipticity. This process is tunable by changing the phase shift applied to the low-frequency modulation signals. The proposed concept has been implemented using a time-modulated square patch antenna that exploits even/odd symmetries to maximize frequency conversion. Simulated and measured results confirm isolation levels over 40 dB in transmission and reception, as well as the ability to generate/receive waves with desired ellipticity and high polarization purity. We expect this antenna to find a wide variety of polarimetric applications, including material analysis, radar, sensing, imaging, and communication systems.

It should be noted that the main goal of this paper was to demonstrate nonreciprocal polarization control, and thus the devices were not fully optimized for other applications. Future antennas will benefit from available techniques based on time-modulation [54], [55] or switched networks [56], [57] to enhance their operational bandwidth and reduce loss while keeping their nonreciprocal nature. Additionally, the proposed concept can be extended to account for any polarization state of the Poincaré sphere. To this purpose, the time-modulated antenna requires the ability to arbitrarily modify the amplitude of each orthogonal surface currents induced in its surface. In the proposed prototype, this can be accomplished by manipulating the 180° phase difference between time-modulated signals aligned along the same direction (x, y). Indeed, it has been demonstrated

that controlling such phase permits to manipulate the intensity of the received/radiated fields [38]. However, this solution increases the prototype complexity by requiring two additional phase shifters and additional control signals. Moving beyond, we envision that future array systems may integrate nonreciprocal antenna elements to obtain fully tailored radiation patterns able to exhibit drastically different responses in both amplitude and polarization while transmitting and receiving electromagnetic waves.

APPENDIX

Fig. 10 describes a dual-fed microstrip patch antenna combined with a 90° hybrid coupler able to achieve circular polarization and to split LHCP and RHCP components [30]–[31]. Figs. 10a-b show the dimensions of the structure and a picture of a prototype, respectively. Port 2 and 3 are associated with the LHCP and RHCP components of the fields, respectively. Fig. 10c shows the measured scattering parameters, confirming excellent matching to free-space and very low cross coupling, whereas Fig. 10d shows the numerically simulated axial ratio.

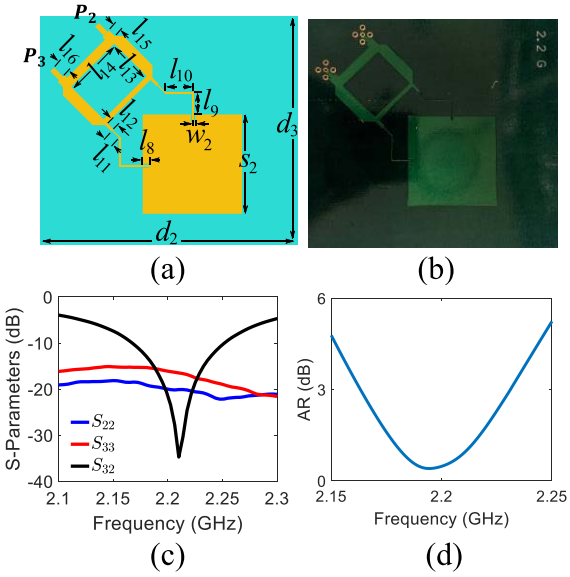

FIGURE 10. Reference antenna composed of a linear and dual-fed patch antenna integrated with a 90° hybrid coupler [30], [31]. Ports 2 and 3 control the LHCP and RHCP component of the radiated waves, respectively. The antenna is printed on a Rogers RT/duroid 5880 substrate with a thickness of 1.575 mm, a relatively dielectric constant of 2.2, and a loss tangent of 0.0009. (a) Antenna schematic and (b) picture of a fabricated prototype. (c) Measured scattering parameters and (d) simulated axial ratio. Antenna dimensions (in mm) are (in mm): $d_2 = 126, d_3 = 116, s_2 = 44, w_2 = 0.5, l_8 = 2, l_9 = 8, l_{10} = 12.2, l_{11} = 6, l_{12} = 4, l_{13} = 21.9, l_{14} = 24.2, l_{15} = 2.2, l_{16} = 5.5$.

ACKNOWLEDGMENT

(James T. S. Do and Jiawei Zang contributed equally to this work.)

REFERENCES

[1] C. Caloz, A. Alù, S. Tretyakov, D. Sounas, K. Achouri, and Z.-L. Deck-Léger, "Electromagnetic nonreciprocity," *Phys. Rev. A, Gen. Phys.*, vol. 10, no. 4, Oct. 2018, Art. no. 047001.

[2] D. L. Sounas and A. Alù, "Non-reciprocal photonics based on time modulation," *Nature Photon.*, vol. 11, no. 12, pp. 774–783, Dec. 2017.

[3] N. A. Estep, D. L. Sounas, J. Soric, and A. Alù, "Magnetic-free non-reciprocity and isolation based on parametrically modulated coupled-resonator loops," *Nature Phys.*, vol. 10, no. 12, pp. 923–927, Nov. 2014.

[4] A. Kord, D. L. Sounas, and A. Alu, "Magnet-less circulators based on spatiotemporal modulation of bandstop filters in a delta topology," *IEEE Trans. Microw. Theory Techn.*, vol. 66, no. 2, pp. 911–926, Feb. 2018.

[5] N. Reiskarimian and H. Krishnaswamy, "Magnetic-free non-reciprocity based on staggered commutation," *Nature Commun.*, vol. 7, no. 1, p. 11217, Sep. 2016.

[6] T. Dinc, A. Nagulu, and H. Krishnaswamy, "A millimeter-wave non-magnetic passive SOI CMOS circulator based on spatio-temporal conductivity modulation," *IEEE J. Solid-State Circuits*, vol. 52, no. 12, pp. 3276–3292, Dec. 2017.

[7] A. Kord, M. Tymchenko, D. L. Sounas, H. Krishnaswamy, and A. Alù, "CMOS integrated magnetless circulators based on spatiotemporal modulation angular-momentum biasing," *IEEE Trans. Microw. Theory Techn.*, vol. 67, no. 7, pp. 2649–2662, Jul. 2019.

[8] S. Taravati, "Self-biased broadband magnet-free linear isolator based on one-way space-time coherency," *Phys. Rev. B, Condens. Matter*, vol. 96, no. 23, p. 35150, Dec. 2017.

[9] D. L. Sounas, J. Soric, and A. Alù, "Broadband passive isolators based on coupled nonlinear resonances," *Nature Electron.*, vol. 1, no. 2, pp. 113–119, Feb. 2018.

[10] X. Wu, X. Liu, M. D. Hickle, D. Peroulis, J. S. Gomez-Diaz, and A. Alvarez-Melcon, "Isolating bandpass filters using time-modulated resonators," *IEEE Trans. Microw. Theory Techn.*, vol. 67, no. 6, pp. 2331–2345, Apr. 2019.

[11] A. Alvarez-Melcon, X. Wu, J. Zang, X. Liu, and J. S. Gomez-Diaz, "Coupling matrix representation of nonreciprocal filters based on time-modulated resonators," *IEEE Trans. Microw. Theory Techn.*, vol. 67, no. 12, pp. 4751–4763, Dec. 2019.

[12] J. Zang, S. Wang, A. Alvarez-Melcon, and J. S. Gomez Diaz, "Nonreciprocal filtering power dividers," *Int. J. Electron. Commun.*, vol. 132, Apr. 2021, Art. no. 153609.

[13] A. Ashley and D. Psychogiou, "RF co-designed bandpass filters/isolators using nonreciprocal resonant stages and microwave resonators," *IEEE Trans. Microw. Theory Techn.*, vol. 69, no. 4, pp. 2178–2190, Apr. 2021.

[14] Z. Wu and A. Grbic, "Serrodyne frequency translation using time-modulated metasurfaces," *IEEE Trans. Antennas Propag.*, vol. 68, no. 3, pp. 1599–1606, Mar. 2020.

[15] L. Zhang, X. Q. Chen, S. Liu, Q. Zhang, J. Zhao, J. Y. Dai, G. D. Bai, X. Wan, Q. Cheng, G. Castaldi, V. Galdi, and T. J. Cui, "Space-time-coding digital metasurfaces," *Nature Commun.*, vol. 9, no. 1, p. 4334, Dec. 2018.

[16] J. Y. Dai, J. Zhao, Q. Cheng, and T. J. Cui, "Independent control of harmonic amplitudes and phases via a time-domain digital coding metasurface," *Light Sci. Appl.*, vol. 7, no. 1, p. 90, Nov. 2018.

[17] J. Zhao, X. Yang, J. Y. Dai, Q. Cheng, X. Li, N. H. Qi, J. C. Ke, G. D. Bai, S. Liu, S. Jin, A. Alù, and T. J. Cui, "Programmable time-domain digital-coding metasurface for non-linear harmonic manipulation and new wireless communication systems," *Nat. Sci. Rev.*, vol. 6, no. 2, pp. 231–238, Nov. 2018.

[18] L. Zhang, X. Q. Chen, R. W. Shao, J. Y. Dai, Q. Cheng, G. Castaldi, V. Galdi, and T. J. Cui, "Breaking reciprocity with space-time-coding digital metasurfaces," *Adv. Mater.*, vol. 31, Oct. 2019, Art. no. 1904069.

[19] M. Liu, D. A. Powell, Y. Zarate, and I. V. Shadrivov, "Huygens' metadevices for parametric waves," *Phys. Rev. X*, vol. 8, no. 3, Sep. 2018, Art. no. 031077.

[20] Y. Hadad, D. L. Sounas, and A. Alu, "Space-time gradient metasurfaces," *Phys. Rev. B, Condens. Matter*, vol. 92, no. 10, Sep. 2015, Art. no. 100304(R).

[21] A. Shaltout, A. Kildishev, and V. Shalaev, "Time-varying metasurfaces and Lorentz non-reciprocity," *Opt. Mater. Exp.*, vol. 5, no. 11, p. 2459, Nov. 2015.

[22] J. W. Zang, D. Correas-Serrano, J. T. S. Do, X. Liu, A. Alvarez-Melcon, and J. S. Gomez-Diaz, "Nonreciprocal wavefront engineering with time-modulated gradient metasurfaces," *Phys. Rev. A, Gen. Phys.*, vol. 11, no. 5, p. 05405, May 2019.

[23] A. E. Cardin, S. R. Silva, S. R. Vardeny, W. J. Padilla, A. Saxena, A. J. Taylor, W. J. M. Kort-Kamp, H.-T. Chen, D. A. R. Dalvit, and A. K. Azad, "Surface-wave-assisted nonreciprocity in spatio-temporally modulated metasurfaces," *Nature Commun.*, vol. 11, no. 1, pp. 1–9, Dec. 2020.

[24] S. Taravati and G. V. Eleftheriades, "Full-duplex nonreciprocal beam steering by time-modulated phase-gradient metasurfaces," *Phys. Rev. A, Gen. Phys.*, vol. 14, no. 1, Jul. 2020, Art. no. 014027.
[25] Z. Wu, C. Scarborough, and A. Grbic, "Space-time-modulated metasurfaces with spatial discretization: Free-space N-path systems," *Phys. Rev. A, Gen. Phys.*, vol. 14, no. 6, Dec. 2020, Art. no. 064060.
[26] X. Wang, A. Díaz-Rubio, H. Li, S. A. Tretyakov, and A. Alù, "Theory and design of multifunctional space-time metasurfaces," *Phys. Rev. A, Gen. Phys.*, vol. 13, no. 4, Apr. 2020, Art. no. 044040.
[27] D. Ramaccia, D. L. Sounas, A. Alu, A. Toscano, and F. Bilotti, "Phase-induced frequency conversion and Doppler effect with time-modulated metasurfaces," *IEEE Trans. Antennas Propag.*, vol. 68, no. 3, pp. 1607–1617, Mar. 2020.
[28] Q. Hu, K. Chen, N. Zhang, J. Zhao, T. Jiang, J. Zhao, and Y. Feng, "Arbitrary and dynamic Poincaré sphere polarization converter with a time-varying metasurface," *Adv. Opt. Mater.*, vol. 10, no. 4, Feb. 2022, Art. no. 2101915.
[29] S. Taravati and G. V. Eleftheriades, "Microwave space-time-modulated metasurfaces," *ACS Photon.*, vol. 9, pp. 305–318, Jan. 2022, doi: 10.1021/acsphotonics.1c01041.
[30] C. A. Balanis, *Modern Antenna Handbook*. Hoboken, NJ, USA: Wiley, 2008.
[31] J. Volakis, *Antenna Engineering Handbook*, 4th ed. New York, NY, USA: McGraw-Hill, 2007.
[32] H.-Y. Yang, J. A. Castaneda, and N. G. Alexopoulos, "Multifunctional and low RCS nonreciprocal microstrip antennas," *Electromagnetics*, vol. 12, no. 1, pp. 17–31, Jan. 1992.
[33] T. Kodera and C. Caloz, "Integrated leaky-wave antenna–duplexer/diplexer using CRLH uniform ferrite-loaded open waveguide," *IEEE Trans. Antennas Propag.*, vol. 58, no. 8, pp. 2508–2514, Aug. 2010.
[34] A. Nagulu, N. Reiskarimian, and H. Krishnaswamy, "Non-reciprocal electronics based on temporal modulation," *Nature Electron.*, vol. 3, no. 5, pp. 241–250, 2020.
[35] Y. Hadad, J. C. Soric, and A. Alù, "Breaking temporal symmetries for emission and absorption," *Proc. Nat. Acad. Sci. USA*, vol. 113, no. 13, pp. 3471–3475, Mar. 2016.
[36] D. Correas-Serrano, J. S. Gomez-Diaz, D. L. Sounas, Y. Hadad, A. Alvarez-Melcon, and A. Alù, "Nonreciprocal graphene devices and antennas based on spatiotemporal modulation," *IEEE Antennas Wireless Propag. Lett.*, vol. 15, pp. 1529–1532, 2016.
[37] S. Taravati and C. Caloz, "Mixer-duplexer-antenna leaky-wave system based on periodic space-time modulation," *IEEE Trans. Antennas Propag.*, vol. 65, no. 2, pp. 442–452, Feb. 2017.
[38] J. W. Zang, A. Alvarez-Melcon, and J. S. Gomez-Diaz, "Nonreciprocal phased-array antennas," *Phys. Rev. A, Gen. Phys.*, vol. 12, no. 5, Nov. 2019, Art. no. 054008.
[39] M. T. Weiss, "Non-reciprocal directive antenna arrays," U.S. Patent US 2 786 999 A, Mar. 26, 1957.
[40] T. Guo, Q. Zhang, A. Kandwal, R. Wang, and Y. Chen, "Design of nonreciprocal antenna array," in *Proc. Int. Workshop Antenna Technol., Small Antennas, Innov. Struct., Appl. (iWAT)*, 2017, pp. 312–315.
[41] J. Zang, X. Wang, A. Alvarez-Melcon, and J. S. Gomez-Diaz, "Nonreciprocal Yagi–Uda filtering antennas," *IEEE Antennas Wireless Propag. Lett.*, vol. 18, no. 12, pp. 2661–2665, Dec. 2019.
[42] R. Karimian, S. Taravati, M. D. Ardakani, S. Ahmadi, and M. E. Zaghloul, "Nonreciprocal-beam phased-array antennas based on transistor-loaded phase shifters," *IEEE Trans. Antennas Propag.*, vol. 69, no. 11, pp. 7572–7581, Nov. 2021.
[43] J. Tinbergen, *Astronomical Polarimetry*. Cambridge, U.K.: Cambridge Univ. Press, 2007.
[44] M. I. Mishchenko, Y. S. Yatskiv, V. K. Rosenbush, and G. Videens, "Polarimetric detection, characterization and remote sensing," in *Proc. NATO Adv. Study Inst. Special Detection Technique (Polarimetry) Remote Sens.*, Yalta, Ukraine, 2010, pp. 1–15.
[45] M. Boerner, "Recent advances in extra-wide-band polarimetry, interferometry and polarimetric interferometry in synthetic aperture remote sensing and its applications," *IEE Proc.-Radar Sonar Navig.*, vol. 150, no. 3, pp. 113–124, 2003.
[46] S. W. Cheung, C. F. Zhou, Q. L. Li, and T. I. Yuk, "A simple polarization-reconfigurable antenna," in *Proc. 10th Eur. Conf. Antennas Propag. (EuCAP)*, Apr. 2016, pp. 1–4, doi: 10.1109/EuCAP.2016.7481801.
[47] P. Pan and B. Guan, "A wideband polarization reconfigurable antenna with six polarization states," in *Proc. 12th Int. Symp. Antennas, Propag. EM Theory (ISAPE)*, Dec. 2018, pp. 1–4, doi: 10.1109/ISAPE.2018.8634224.
[48] A. Panahi, X. L. Bao, K. Yang, O. O'Conchubhair, and M. J. Ammann, "A simple polarization reconfigurable printed monopole antenna," *IEEE Trans. Antennas Propag.*, vol. 63, no. 11, pp. 5129–5134, Nov. 2015, doi: 10.1109/TAP.2015.2474745.
[49] H. L. Zhu, S. W. Cheung, X. H. Liu, and T. I. Yuk, "Design of polarization reconfigurable antenna using metasurface," *IEEE Trans. Antennas Propag.*, vol. 62, no. 6, pp. 2891–2898, Jun. 2014, doi: 10.1109/TAP.2014.2310209.
[50] C. Ni, M. S. Chen, Z. X. Zhang, and X. L. Wu, "Design of frequency-and polarization-reconfigurable antenna based on the polarization conversion metasurface," *IEEE Antennas Wireless Propag. Lett.*, vol. 17, no. 1, pp. 78–81, Jan. 2018, doi: 10.1109/LAWP.2017.2775444.
[51] J.-S. Row, W.-L. Liu, and T.-R. Chen, "Circular polarization and polarization reconfigurable designs for annular slot antennas," *IEEE Trans. Antennas Propag.*, vol. 60, no. 12, pp. 5998–6002, Dec. 2012, doi: 10.1109/TAP.2012.2211556.
[52] M. A. Bourkov, J. Do, X. Liu, A. Alvarez-Melcon, and J. S. Gomez-Diaz, "Time-modulated patch antennas with nonreciprocal polarization handedness," in *Proc. IEEE Int. Symp. Antennas Propag. North Amer. Radio Sci. Meeting*, Jul. 2020, pp. 745–746.
[53] J. Zang, E. Carrasco, X. Wang, A. Alvarez-Melcon, and J. S. Gomez-Diaz, "Analysis and design of true-time delay reflectarray antennas: A filter perspective," *IEEE Access*, vol. 8, pp. 44947–44956, 2020.
[54] A. Kord, D. L. Sounas, and A. Alù, "Low-loss broadband magnetless circulators for full-duplex radios," in *IEEE MTT-S Int. Microw. Symp. Dig.*, Jun. 2018, pp. 506–509.
[55] A. Kord, D. L. Sounas, Z. Xiao, and A. Alù, "Broadband cyclic-symmetric magnetless circulators and theoretical bounds on their bandwidth," *IEEE Trans. Microw. Theory Techn.*, vol. 66, no. 12, pp. 5472–5481, Dec. 2018.
[56] A. Nagulu, T. Dinc, Z. Xiao, M. Tymchenko, D. L. Sounas, A. Alù, and H. Krishnaswamy, "Nonreciprocal components based on switched transmission lines," *IEEE Trans. Microw. Theory Techn.*, vol. 66, no. 11, pp. 4706–4725, Nov. 2018.
[57] M. Tymchenko, D. Sounas, A. Nagulu, H. Krishnaswamy, and A. Alù, "Quasielectrostatic wave propagation beyond the delay-bandwidth limit in switched networks," *Phys. Rev. X*, vol. 9, no. 3, Jul. 2019, Art. no. 031015.

JAMES T. S. DO received the B.S. degree in electrical engineering from Purdue University, in 2006, the M.E. degree in electrical engineering from the University of Virginia, in 2013, and the Ph.D. degree in electrical engineering from the University of California at Davis, in 2019. Previously, he was the Lead RF Engineer with the Custom Systems Department, Virginia Diodes Inc., from 2008 to 2014, where he designed and tested systems and components operating up to 3 THz, including the world's first 1 THz vector network analyzer extension module. He is currently a Consultant at Virginia Diodes Inc., where he is designing the next generation of THz Schottky diode mixers and frequency multipliers. He is also a Research Collaborator at the University of California at Davis. His current research interests include the development of devices, such as mixers and frequency multipliers, nonreciprocal components based on time modulation, and microwave filters.

JIAWEI ZANG (Member, IEEE) received the Ph.D. degree in electrical engineering from the Beijing Institute of Technology, Beijing, China, in 2019.

From September 2017 to November 2018, he was a Visiting Student with the Department of Electrical and Computer Engineering, University of California at Davis. He is currently with the China Academy of Information and Communications Technology, Beijing. His research interests include antennas, filters, and nonreciprocal components.

ALEJANDRO ALVAREZ-MELCON (Senior Member, IEEE) was born in Madrid, Spain, in 1965. He received the bachelor's degree in telecommunications engineering from the Technical University of Madrid (UPM), Madrid, in 1991, and the Ph.D. degree in electrical engineering from the Swiss Federal Institute of Technology Lausanne, Switzerland, in 1998.

In 1988, he joined the Signal, Systems and Radio Communications Department, UPM, as a Research Student, where he was involved in the design, testing, and measurement of broad-band spiral antennas for electromagnetic measurements support (EMS) equipment. From 1991 to 1993, he was with the Radio Frequency Systems Division, European Space Agency (ESA/ESTEC), Noordwijk, The Netherlands, where he was involved in the development of analytical and numerical tools for the study of waveguide discontinuities, planar transmission lines, and microwave filters. From 1993 to 1995, he was with the Space Division, Industry Alcatel Espacio, Madrid, and the ESA, where he collaborated in several ESA/European Space Research and Technology Centre (ESTEC) contracts. From 1995 to 1999, he was with the Swiss Federal Institute of Technology, Ecole Polytechnique Federale de Lausanne (EPFL), Lausanne, where he was involved in the field of microstrip antennas and printed circuits for space applications. In 2000, he joined the Technical University of Cartagena, Spain, where he is currently developing his teaching and research activities. He was an Invited Professor with the Polytechnique Montréal, Canada, from July 2010 to September 2010, and a Visiting Professor with the University of California at Davis, USA, from October 2017 to September 2018.

Dr. Alvarez-Melcon was a recipient of the Journee Internationales de Nice Sur les Antennes (JINA) Best Paper Award for the best contribution to the JINA 98 International Symposium on Antennas and the Colegio Oficial de Ingenieros de Telecomunicacion (COIT/AEIT) Award to the Best Ph.D. Dissertation in basic information and communication technologies.

JUAN SEBASTIAN GOMEZ-DIAZ (Senior Member, IEEE) was born in Ontur, Spain. He received the M.Sc. and Ph.D. degrees in electrical engineering from the Technical University of Cartagena, Cartagena, Spain, in 2006 and 2011, respectively.

During the development of the Ph.D. degree, he held a visiting research positions with the École Polytechnique de Montréal, Canada, and the Fraunhofer Institute for High Frequency Physics and Radar Techniques, Germany. From October 2011 to March 2014, he was a Postdoctoral Fellow with the École Polytechnique Fédéral de Lausanne (EPFL), Switzerland. From May 2014 to August 2016, he continued his postdoctoral work with the Metamaterials and Plasmonic Research Laboratory, The University of Texas at Austin. He is currently an Associate Professor with the Electrical and Computer Engineering Department, University of California at Davis. His research interests include multidisciplinary areas of electromagnetic wave propagation and radiation, metamaterials and metasurfaces, plasmonics, 2D materials, nonreciprocal and nonlinear phenomena, and other emerging topics on applied electromagnetics and nanotechnology.

Dr. Gomez-Diaz was a recipient of the Keck Foundation Award, the NSF CAREER Award, the 2017 Leopold Felsen Award for Excellence in Electrodynamics, the Raj Mittra Award presented by the 2015 IEEE Antennas and Propagation Society, the Young Scientist Award of the 2015 URSI Atlantic RadioScience Conference, the FP7 Marie Curie Fellowship from the European Commission, in 2012, the Colegio Oficial de Ingenieros de Telecomunicación (COIT/AEIT) Award to the Best Spanish Ph.D. thesis in basic information and communication technologies, in 2011, and the Best Ph.D. Thesis Award from the Technical University of Cartagena. He serves as a reviewer for several journals on antennas, microwaves/terahertz, and physics.